

2014 中華民國航太學會學術研討會論文投稿封頁

A. 論文資料：

論文題目：Low Speed Wind Tunnel Study of Variable Tandem Wing Aircraft
Design: Earlier-on Experiment and Study

論文類別： 1, 6

徵文範圍 (類別) 編號

1. 空氣動力學	2. 實驗與計算流體力學	3. 燃燒與熱質傳	4. 噴射推進與渦輪引擎	5. 航太結構及先進材料
6. 飛行力學	7. 航太電子及通訊	8. 飛行控制與導引	9. 全球定位系統	10. 天體力學
11. 旋翼機	12. 無人飛行載具	13. 微奈系統科技	14. 航太實驗設備與測試	15. 航太系統與次系統
16. 航太製造及維修	17. 衛星系統工程	18. 適航認證	19. 民航法規與制度	20. 飛航及安全管理
21. 航空資訊技術	22. 航空經濟與財務	23. 民航飛行技術	24. 空域規劃與管理	25. 航太醫學
26. 航空保安	27. 航空運輸與環境	28. 航太品保	29. 航太科技教育	30. 其他航太相關應用

作者 (中文)：王培儒、鄭子暘、蔣小偉教授

作者 (英文)：Peir-Ru Wang, Zi-Yang Zheng, Pro. Hsiao-Wei Chiang

若投稿論文為科技部研究計畫之成果，請註明科技部計畫編號：

連絡人：王培儒

單位：國立清華大學動力機械系

B. 論文競賽：每篇論文均須勾選一項

本論文 參加『學生論文競賽』

不參加『學生論文競賽』

Low Speed Wind Tunnel Study of Variable Tandem Wing Aircraft Design: Earlier-on Experiment and Study

可變串列翼在低速下的特性：先期實驗與初探

Wang, Peir-Ru (王培儒)

Student, Department of Power Mechanical Engineering, National Tsing Hua University

Zheng, Zi-Yang (鄭子暘)

Student, Department of Power Mechanical Engineering, National Tsing Hua University

Chiang, Hsiao-Wei (蔣小偉 教授)

Professor, Department of Power Mechanical Engineering, National Tsing Hua University

Abstract

This research is to find the characteristics of tandem wings in different configurations. We used an existing wind tunnel which was designed for wind turbines tests. We measured the flow field of the wind tunnel and chose the test section. A three-force balance device was designed for the test. Then we assembled the 3D printing model single wing on the three-force balance and put in the wind tunnel to establish the baseline data. The results agreed well with the theory. For the experiments on tandem wing, as we decrease the distance between the front and rear wings, the expected lift increase becomes smaller. It demonstrated that the lift decrease is due to the rear wing lift affected by the vortices shedding from the front wing.

Keywords : Tandem wing, low speed, wind tunnel

1 Motivation

The idea came from the US Air force report “Energy Horizons” in 2012. In page 10, it proposed:

... Similarly, center of gravity (CG) controls and lift distribution control systems enhance performance by ensuring lift is efficiently appropriated across the aircraft in relation to the location of the carried weight.

How to ensure lift is efficiently across the gravity centroid? This question makes us to construct a new model to research and analyze the behavior of our model.

Recently, there are some aircraft which can change the position of lift like F-14, B-1, Tu-160, etc. Precisely, those aircraft with variable-sweep wing actually is to increase the critical speed and raise the low speed control ability. When aircraft approach critical speed, 0.8 Mach number, so-called transonic, airflow on the wing will reach sonic speed and

generate shock waves. The result of shock waves will include higher drag and control difficulty. In order to solve it, the answer is swept wing. Most aircraft used backward swept wing to increase critical speed. If designer designs a high swept angle wing, it will cause the divergence of air flow and make it difficult to control in low speed such as landing. Some aircraft like Convair B-58 with delta wing has very high landing speed and cause many crashes. As a result, variable-sweep wing can be a great answer for this problem.

Although the variable-sweep wing gives aircraft higher control ability, it also causes the disadvantage of lift moving backward. When wings sweep back, lift will move back and cause pitching moment. Then the empennage must get involved to balance the moment. The balanced force will cause more drag and less fuel efficiency.

At first we proposed two designs. The first

design is illustrated as Fig. 1-1, which has a movable and variable wing to change the position of lift. But Fig. 1-1 shows that it may cause too large load on the changeable mechanism and be too complex, we proposed the second design as Fig. 1-2. In Fig. 1-2 is a tandem wing design aircraft. The front wing is a variable swept angle design and the other is a changeable position wing. We chose the second design for this paper.

Then we started to design our test model. The model plane needs to have the design to change configuration. The model shown in Fig. 3-1 displays the ability to remove, add, or change the position of the wings.

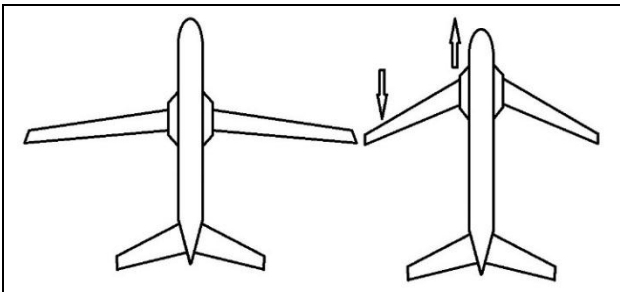


Fig. 1-1. First design.

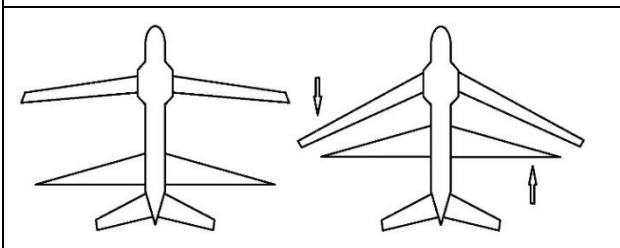


Fig. 1-2. Second design.

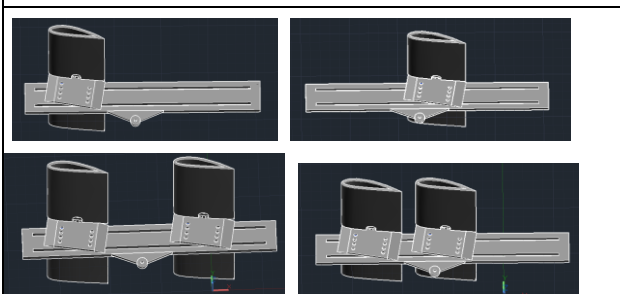


Fig. 1-3. Plane model shows the ability to change configuration.

2 Nomenclature

⊕ : It means the counterclockwise is positive

D : Total drag of the model plane.

d: The leg length of the three-force balance.

$D_{1,2,3}$: drag of three-force balance and scales.

F_1 : The force detect by scale 1.

F_2 : The force detect by scale 2.

F_3 : The force detect by scale 3.

F_{23} : F_{23} is the sum of F_2 and F_3 .

h: equivalent position of the plane drag(see Fig. 7-1)

L: Total lift force, equal to the sum of F_1 , F_2 and F_3 .

L_{bw} : Lift force generated by the front wing.

L_{fw} : Lift force generated by the rear wing.

n_1 : Coefficient of the front wing lift position.

n_2 : Coefficient of the rear wing lift position.

r_1, r_2 : Length of the three-force balance.

S: Length of the stick on the three-force balance.

X_1 : Front wing trailing edge to middle plane body.

X_2 : Rear wing trailing edge to middle plane body.

Greeks:

$\Delta F_1, \Delta F_{23}$: F_1 and F_{23} change as X_1 change to $X_1 + \Delta x$.

Δx : The change quantity of position X_1 .

θ : The angle to set the three-force balance.

λ : Chord length of the plane model.

$\Sigma F_x, \Sigma F_y$: Net force on X-axis, Y-axis.

ΣM_{O1} : Moment with respect to O1

ΣM_{O2} : moment with respect to O2

3 Test Model

We used 3D printing to make our wing model. We chose NACA4418 with chord length of 6cm. At first we set 0 degree as the angle of attack, but the lift was too weak (~4g) and the noise caused by wing vibration made it hard to analyze. Then we increase the angle of attack to 9 degrees (also shown in Fig. 1-3), the lift (~13g) became three times larger than the 0 degree case. The vibration noise became relatively smaller so we were able to record and analyze the data.

We used 3M tape to keep the surface smooth in order to reduce turbulence. The wings were designed hollow to avoid shrinking during printing. We also sealed up the wing tips to avoid turbulence. Fig. 3-1 shows that we smooth out the sharp corners to avoid turbulence generation.

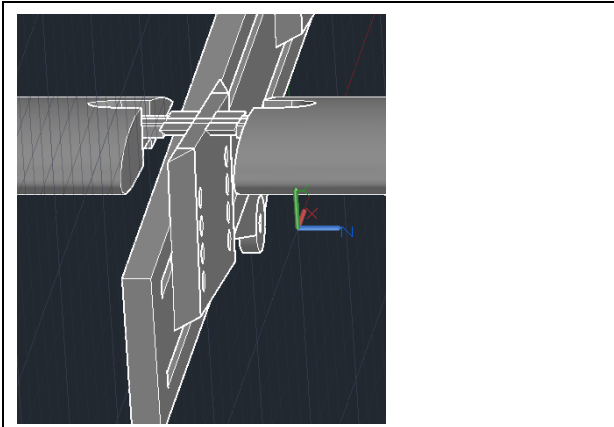


Fig. 3-1 Smooth corners to avoid turbulence

4 Wind Tunnel Flow Field Measurement

In order to studying the effects of air moving past the wing, we put the model into the wind tunnel. With fan and measurement equipment, we can get the data from our model, including lift force and drag force. The first step, we need to measure the flow field in the tunnel. Then we can choose the test section which has more stable and stronger wind.

We use a Hot-Wire Anemometer to measure the wind speed in the wind tunnel. With the fan rotational frequency at 30Hz, the Hot-Wire measured the wind speed to be 2.4m/s to 4.8m/s. Fig. 4-1 showed the speed in the middle is weaker because of the spindle of fan. The wind speed on the edge of the tunnel is also weak. The upper middle of the tunnel is relative strong and uniform. Therefore, we decided to choose the upper middle part in the wind tunnel as the test section for the model.

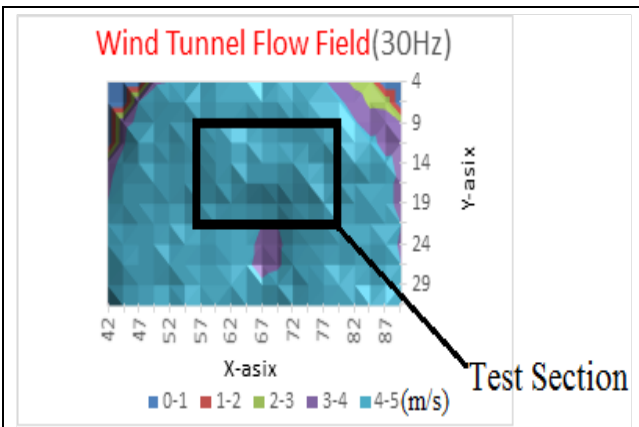


Fig. 4-1. The flow field of the fan rotational frequency at 30Hz.

After deciding the area where the wing will be set up, we can reduce the measured range of wind speed in the tunnel. The second time, we adjust the measurement of range. In order to increase the Reynolds number of the model, we increased the rotational frequency to 40Hz. Using the Hot-Wire Anemometer to measure the speed of wind, Fig. 4-2 showed the range of speed is about 5m/s to 6.2m/s.

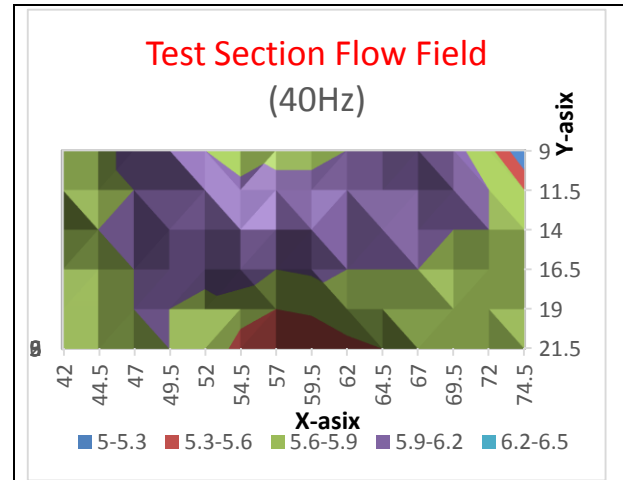


Fig. 4-2 The flow field of test section when the fan is rotating at 40Hz.

5 Three-Force Balance Device

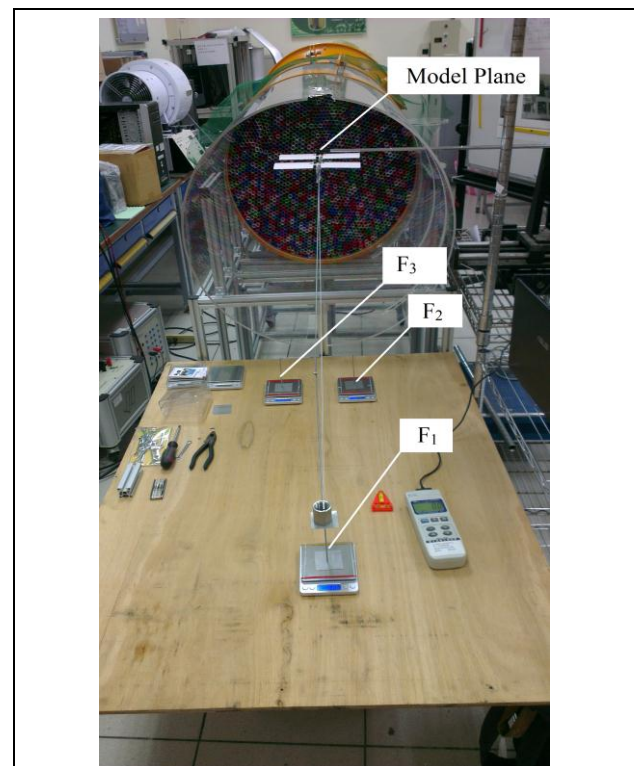


Fig. 5-1. Three-force balance device.

Fig. 5-1 shows the outline of the three-force balance. The scale in front of the photo is F_1 scale, and the other two scales are F_2 and F_3 . The sum of F_1 , F_2 , and F_3 is equal to the lift. More details will be introduced in the following paragraph.

6 Experiments and Data Acquisition

6.1 Method of experiment

We moved the wings to the specific position and stick a bubble level on the model. It can maintain the level of model and the angle of attack. We also put a small stick with cotton thread at the front of the model. Once we put the model into the wind tunnel, we can see whether the cotton thread floating in the wind is in parallel with the model or not. As a result, we can ensure the model is straight in the wind tunnel.

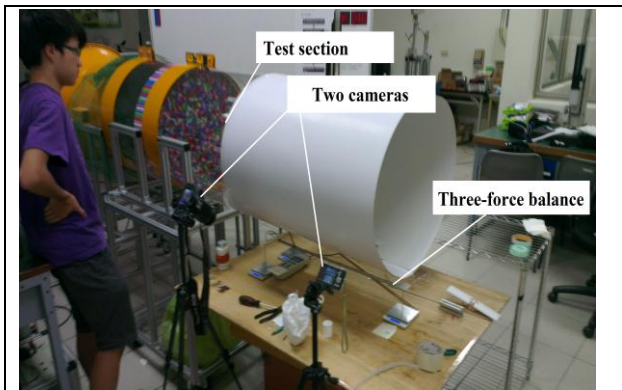


Fig. 6-1. Data measurements.

The equipment of our experiment is a three force balance. We put three electronic scales under the legs of three-force balance. Then we put the model and the support of three force balance into the wind tunnel. Before starting the experiment, we turned on the wind tunnel, slightly perturb the three force balance and let the value of F_2 and F_3 be checked, then we turn off the wind tunnel. Until the model is stable, we press the switches of the three electronic sales at the same time and turn on wind tunnel to start the experiment. Two digital cameras were in place to record the three electronic scales. We also use Hot-Wire to measure the wind speed and temperature to ensure the temperature is stable during the experiment, since the wind speed is also affected by the temperature.

6.2 Data Acquisition

Ulead VideoStudio was used to read the camera film. As a “1st method”, we recorded the data of the electronic scales for 20 seconds including F_1 , F_2 , F_3 , temperature, and wind speed per second, thus we have 20 samples in total.



Fig. 6-2. The screenshot shows the way for record the scale quantity of three-force balance.

Soon we noticed that the arbitrary time interval we chose may cause errors. In order to obtain more accurate result, as a “2nd method”, we recorded the data for 93 seconds with 93 samples. It must be more representative than the 20 sample data. Although “2nd method” would be more accurate, it will take us much more time to deal with the heavy data. In Fig. 6-3, the average data of F_1 versus time will have less than 3% errors in different time intervals.

Therefore, we decided to try the “3rd method”. We still take 20 samples but changing from taking one sample per second to taking one sample every five seconds. Then we acquire five groups of data, i.e. (1,6,11,16...), (2,7,12,17...), (3,8,13,18...), (4,9,14,19...), and (5,10,15,20...). For each group, we checked all the samples, and we found the above 5 groups’ average values are less than 1% of errors, as comparing with the average of 93 samples in Table. 1.

On the other hand, we used the 93sec data (“2nd method”) as the standard database. First we used “1st method” to choose 5 groups of data with different 20 second intervals, and then we used “3rd method” to choose another 5 groups of data. In Table. 1, we compared the errors between the three methods. We

found all groups of “3rd method” are within the errors of 1% as comparing with the average of 93 samples. Therefore, we used the “3rd method” as our data acquisition approach thereafter.

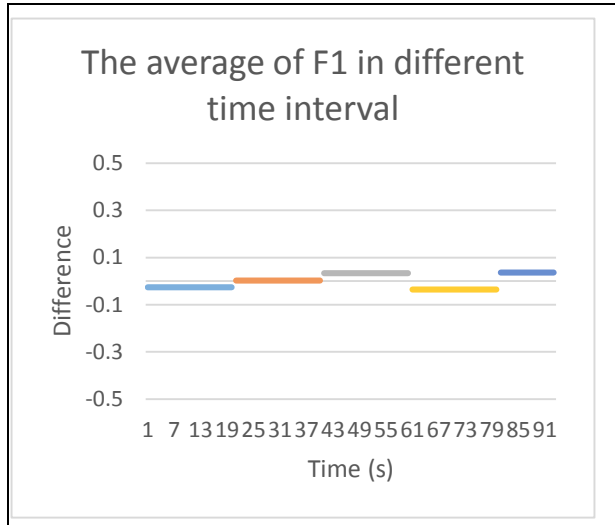


Fig. 6-3 “1st method” caused errors in different time intervals.

7 Basic Method of Analysis

The simple static calculation is essential. As in Fig. 7-1, when the system is in static balance, the sum of all forces and moments are equal to zero. We can easily write 4 equations: net force equal to 0 on X-axis (Eq. 7-1), net force equal to 0 on Y-axis (Eq. 7-2), moment with respect to O₁ equal to 0 (Eq. 7-3), and moment with respect to O₂ equal to 0 (Eq. 7-4).

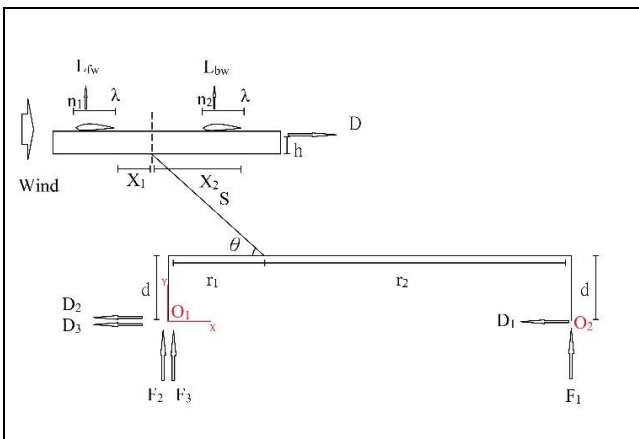


Fig. 7-1. Static balance.

$\Sigma F_x=0:$	$D=D_1+D_2+D_3$	Eq. 7-1
$\Sigma F_y=0:$		

$L_{fw} + L_{bw} + F_1 + F_2 + F_3 = 0$	Eq. 7-2
$\Sigma M_{O1}=0 : \oplus$	
$-L_{fw} \cdot (S \cdot \cos\theta - r_1 + X_1 + \lambda - n_1\lambda)$	
$-L_{bw} \cdot (S \cdot \cos\theta - r_1 + X_2 + \lambda - n_2\lambda)$	
$-D \cdot (h + S \cdot \sin\theta + d) + F_1 \cdot (r_1 + r_2) = 0$	Eq. 7-3
$\Sigma M_{O2}=0 : \oplus$	
$-L_{fw} \cdot (S \cdot \cos\theta + r_2 + X_1 + \lambda - n_1\lambda)$	
$-L_{bw} \cdot (S \cdot \cos\theta + r_2 + X_2 + \lambda - n_2\lambda)$	
$-D \cdot (h + S \cdot \sin\theta + d) - F_{23} \cdot (r_1 + r_2) = 0$	Eq. 7-4

Eq. 7-1 will not be used because we can't measure the quantity of drag. In the future, we may solve this deficiency and it will be mentioned later.

Eq. 7-3 and Eq. 7-4 can be rewritten as:

Eq. 7-3:	
$-(L_{fw} + L_{bw}) \cdot (S \cdot \cos\theta - r_1 + \lambda)$	
$-L_{fw} \cdot (X_1 - n_1\lambda) - L_{bw} \cdot (X_2 - n_2\lambda)$	
$-D \cdot (h + S \cdot \sin\theta + d) + F_1 \cdot (r_1 + r_2) = 0$	Eq. 7-5
Eq. 7-4:	
$-(L_{fw} + L_{bw}) \cdot (S \cdot \cos\theta - r_1 + \lambda)$	
$-L_{fw} \cdot (X_1 - n_1\lambda) - L_{bw} \cdot (X_2 - n_2\lambda)$	Eq. 7-6
$-D \cdot (h + S \cdot \sin\theta + d) - F_{23} \cdot (r_1 + r_2) = 0$	

In our previous experience, we use single wing to build up the data base. Eq. 7-5 and Eq. 7-6 can be reduced to the single wing form:

Eq. 7-5:	
$-L_{fw} \cdot (S \cdot \cos\theta - r_1 + \lambda) - L_{fw} \cdot (X_1 - n_1\lambda)$	
$-D \cdot (h + S \cdot \sin\theta + d) + F_1 \cdot (r_1 + r_2) = 0$	Eq. 7-7
Eq. 7-6:	
$-L_{fw} \cdot (S \cdot \cos\theta - r_1 + \lambda) - L_{fw} \cdot (X_1 - n_1\lambda)$	Eq. 7-8
$-D \cdot (h + S \cdot \sin\theta + d) - F_{23} \cdot (r_1 + r_2) = 0$	

Furthermore, if the wing moves a distance Δx , i.e., the position changes from X_1 to $X_1 + \Delta x$, F_1 and

F_{23} will also be increased to $F_1+\Delta F_1$ and $F_{23}+\Delta F_{23}$. If we assume that the position change of wings doesn't affect lifts, drags, and others, the changes of X_1 , F_1 , F_{23} still satisfy Eq. 7-7 and Eq. 7-8 because of static balance. We substitute into Eq. 7-7 and Eq. 7-8:

<p>Eq. 7-7:</p> $-L_{fw} \cdot (S \cdot \cos\theta - r_1 + \lambda) - L_{fw} \cdot (X_1 + \Delta x - n_1 \lambda) - D \cdot (h + S \cdot \sin\theta + d) + (F_1 + \Delta F_1) \cdot (r_1 + r_2) = 0$ <p style="text-align: right;">[] equal to 0</p> $\rightarrow [-L_{fw} \cdot (S \cdot \cos\theta - r_1 + \lambda) - L_{fw} \cdot (X_1 - n_1 \lambda) - D \cdot (h + S \cdot \sin\theta + d) + F_1 \cdot (r_1 + r_2)] - L_{fw} \cdot \Delta x + \Delta F_1 \cdot (r_1 + r_2) = 0$ <p style="text-align: right;">Eq. 7-9</p> $\therefore -L_{fw} \cdot \Delta x + \Delta F_1 \cdot (r_1 + r_2) = 0$	
<p>Eq. 7-8:</p> $-L_{fw} \cdot (S \cdot \cos\theta - r_1 + \lambda) - L_{fw} \cdot (X_1 + \Delta x - n_1 \lambda) - D \cdot (h + S \cdot \sin\theta + d) - (F_{23} + \Delta F_{23}) \cdot (r_1 + r_2) = 0$ <p style="text-align: right;">[] equal to 0</p> $\rightarrow [-L_{fw} \cdot (S \cdot \cos\theta - r_1 + \lambda) - L_{fw} \cdot (X_1 - n_1 \lambda) - D \cdot (h + S \cdot \sin\theta + d) - F_{23} \cdot (r_1 + r_2)] - L_{fw} \cdot \Delta x - \Delta F_{23} \cdot (r_1 + r_2) = 0$ <p style="text-align: right;">Eq. 7-10</p> $\therefore -L_{fw} \cdot \Delta x - \Delta F_{23} \cdot (r_1 + r_2) = 0$	

Eq. 7-9 and Eq. 7-10 can be used in data analysis.

Using arbitrary chosen data of lift, F_1 , F_{23} , X_1 , we can use these equations to predict and check the correctness of other data.

8 Results

8.1 Single Wing with 20cm Wingspan

The first experiment is the single wing case in order to establish the base line. Then we can use this data to compare with the double length wingspan and tandem wings. We moved the wing position X_1 from 6cm to 9 positions, i.e. 5cm, 4cm, 3cm, 0cm, -3cm, -6cm, -9cm, and -10cm.

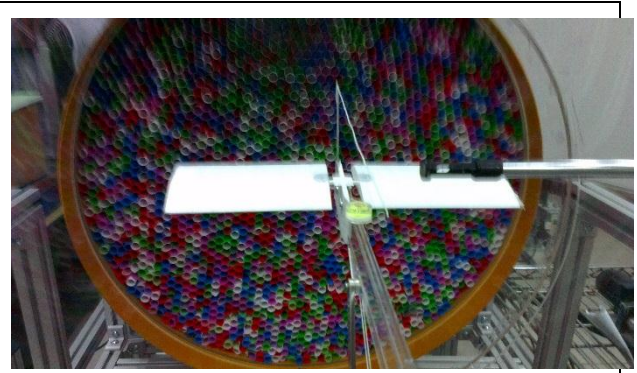


Fig. 8-1. Single wing configuration test.

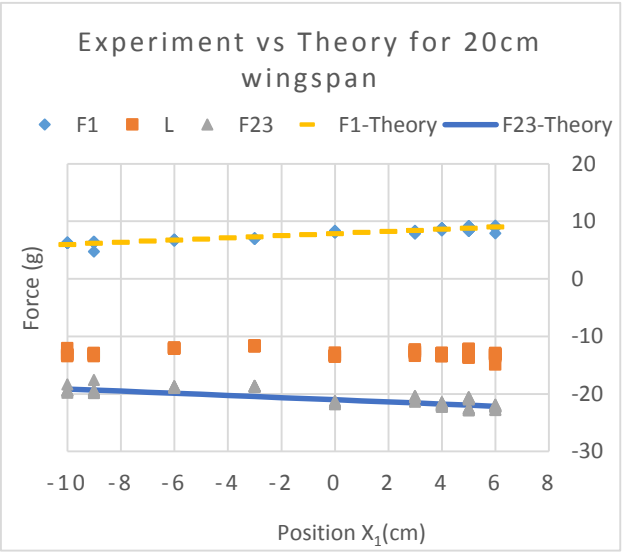
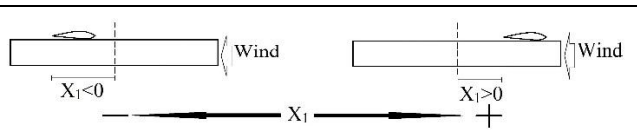


Fig. 8-2 Experimental data versus theory.

Fig. 8-2 shows all the points from -10cm to 6cm. We can see F_1 increases from -10cm to 6cm, and F_{23} decreases from -10cm to 6cm.

Lift force is the sum of F_1 and F_{23} . Fig. 8-2 shows lift forces are almost unchanged as we expected, since the angle of attack is unchanged.

In order to compare the experimental data with theory, we use the 6cm point data, as F_1 , L and F_{23} , into Eq. 7-9 and Eq. 7-10 to obtain the ideal value of other F_1 and F_{23} in different positions. As shown in Fig. 8-2, the experimental data agrees well with the theory, with errors of F_1 6% and F_{23} 10%.

8.2 Single Wing with 40cm Wingspan

Because we will add another pair of wings for

tandem design and thereby doubling the wing area, in order to compare the two, we also need to study the wing area effects by increasing the 20cm single wingspan to 40cm.



Again, we moved the 40cm wing from X_1 at 6cm to 3cm, 0cm, -3cm, -6cm, and -9cm.

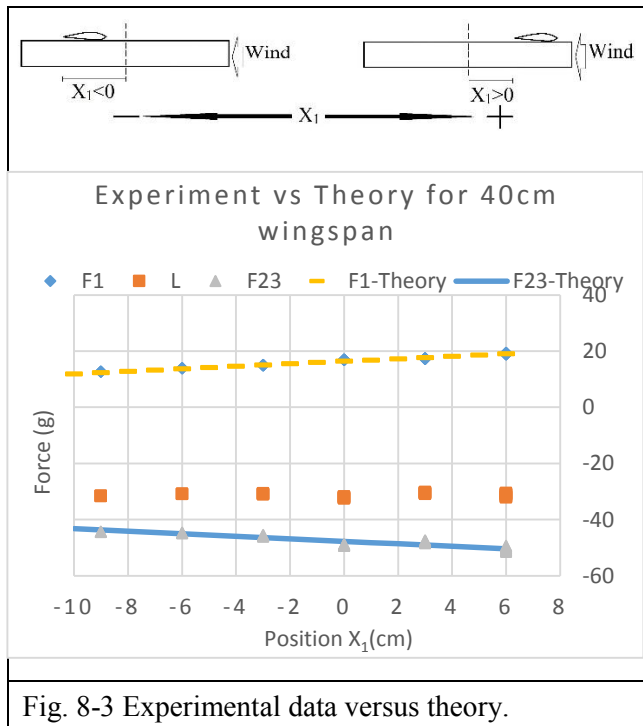


Fig. 8-3 Experimental data versus theory.

Fig. 8-3 shows the distribution of the 40cm results. Eq. 7-9 and Eq. 7-10 are used to predict the theoretical F_1 , F_{23} , and L versus the change of X_1 .

As shown in Fig. 8-3, the experimental data agrees well with the theory, with the 40cm wingspan results even better than the 20cm case.

The average lift of 40cm wingspan is 30g, as compared to the 20cm case of 13g. Other words, the 40cm case lift per span is higher than the 20cm case. It demonstrates that the aircraft with higher aspect ratio wings will have large lift.

8.3 Tandem Wing with 20cm Wingspan

For the tandem wing case, we set both wings on the same horizon. Then we fixed the front wing at $X_1=6$ cm and changing the rear wing position from $X_2=0$ cm, to -3cm, -6cm and -9cm.



Fig. 8-4 Front wing at $X_1=6$ cm and the rear wing at position $X_2=0$ cm.

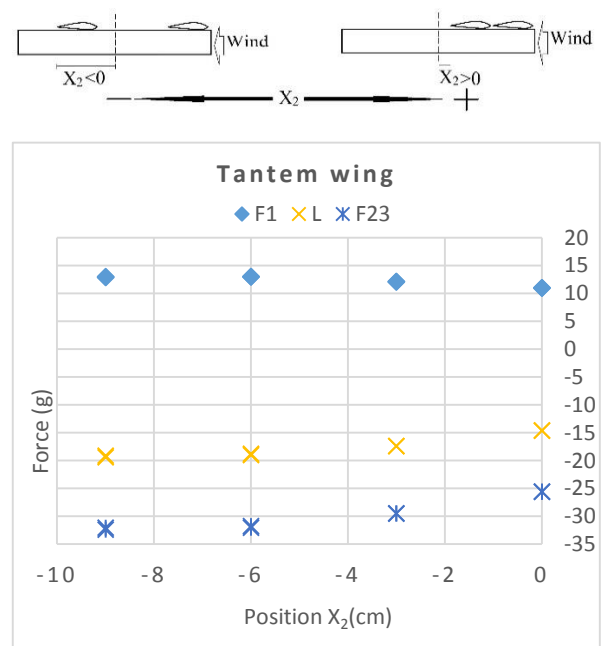


Fig. 8-5 Data distribution of tandem wing case.

As shown in Fig. 8-5, the lift of the tandem wing design is reduced to 15g as we move the rear wing closer to the front wing, which is close to the single 20cm wing case. It was demonstrated that the lift decrease is due to the rear wing lift affected by the vortices shedding from the front wing as they are coming closer. However, as we move the two wings apart, the combined lift can only reach 20g as compared to 30g from the 40cm single wing case.

9 Conclusion

In this study, we set up a wind tunnel and use Hot-Wire Anemometer to find the wind tunnel flow field. We designed a three force balance and use 3D printing to print the model plane wings. In the data acquisition, we found that using the method that taking one sample every five seconds is more accurate than taking one sample every second. The experimental results matched quite well with theory.

In the tandem wing case, it was demonstrated that the

lift decrease is due to the rear wing lift affected by the vortices shedding from the front wing as they are coming closer. As we move the two wings apart, the combined lift can only reach 20g as compared to 30g from the 40cm single wing case. In the future, we will continue the tandem wing experiments by changing the angles of attack for both the front and rear wings as well as the gaps in-between.

4cm-4	Average	1 datum per 1sec and last 20sec (1 st method)					1 datum per 5sec (3 rd method)				
Time interval	93sec	1~20	21~40	41~60	61~80	80~93	1~6...	2~7...	3~8...	4~9...	5~10...
F1 ave in the interval	8.644946237	8.6195	8.6475	8.679	8.61	8.68154	8.64889	8.64222	8.62611	8.64667	8.65167
F2 ave in the interval	-10.31924731	-10.213	-10.289	-10.442	-10.274	-10.41	-10.293	-10.288	-10.339	-10.294	-10.345
F3 ave in the interval	-11.49215054	-11.319	-11.492	-11.565	-11.478	-11.67	-11.497	-11.465	-11.447	-11.47	-11.531
L ave in the interval	-13.16645161	-12.912	-13.134	-13.328	-13.142	-13.398	-13.141	-13.111	-13.161	-13.118	-13.224
Difference between F1 93sec-ave (%)		-0.29%	0.03%	0.39%	-0.40%	0.42%	0.05%	-0.03%	-0.22%	0.02%	0.08%
Difference between F2 93sec-ave (%)		1.03%	0.29%	-1.19%	0.44%	-0.88%	0.26%	0.30%	-0.20%	0.24%	-0.25%
Difference between F3 93sec-ave (%)		1.51%	0.00%	-0.63%	0.13%	-1.55%	-0.04%	0.24%	0.39%	0.19%	-0.33%
Difference between L 93sec-ave (%)		1.93%	0.25%	-1.23%	0.19%	-1.76%	0.19%	0.42%	0.04%	0.37%	-0.44%

Table. 1

10 Reference:

- [1] "Energy Horizons," United States Air Force Energy S&T Vision 2011-2026, AF/ST TR 11-01, 31 January 2012
- [2] Ira Herbert Abbott and Albert E. Von Doenhoff, "Theory of Wing Sections", New York : Dover, 1959.
- [3] "Introduction to flight", John D. Anderson, Jr., New York : McGraw-Hill, c1989.
- [4] "Fundamentals of flight", Richard S. Shevell., Englewood Cliffs, N.J. : Prentice Hall, c1989.
- [5] "Low-speed wind tunnel testing", Pope, Alan, New York : Wiley, c1984.
- [6] "Experimental Investigation on the Aerodynamic Characteristics of a Tandem Wing Configuration in Close Ground Proximity", Mohammed Rafiuddin AHMED and Yasuaki KOHAMA, JSME international journal. Ser. B, Fluids and thermal engineering 42(4), 612-618, 1999-11-15
- [7] San-Yih Lin, Yan-Shin Chin, and Yuh-Ying Wang. "Numerical investigations on two-dimensional canard-wing aerodynamic interference", Journal of Aircraft, Vol. 31, No. 3 (1994), pp. 672-679.